Published by IOP Publishing for Sissa Medialab

Received: *December 9, 2019*
Revised: *February 12, 2020*
Accepted: *March 6, 2020*
Published: *March 31, 2020*

Development of a TDC-based digital positron annihilation lifetime spectrometer

J.J. Ge, Z.W. Xue, L.H. Cong and H. Liang[1]

Department of Modern Physics, University of Science and Technology of China, Hefei 230026, China
State Key Laboratory of Particle Detection and Electronics, University of Science and Technology of China, Hefei 230026, China

E-mail: simonlh@ustc.edu.cn

Abstract: Positron Annihilation Lifetime (PAL) spectroscopyis widely applied in material and biomedical science. The conventional analog PAL spectrometer built by multiple Nuclear Instrumentation Modules gradually shows deficiencies in performance. Most digital PAL spectrometers strongly rely on the advanced Analog-to-Digital Converter (ADC) or oscilloscope with an ultra-high-speed sampling rate. In this paper, we developed a prototype system of the digital PAL spectrometer based on ordinary Time-to-Digital Converter (TDC) and ADC. Benefiting from the high-performance digitization devices and digital signal processing algorithms accomplished by Field-Programmable Gate Array (FPGA), the system achieves remarkable energy and lifetime resolution in a simple structure and at a much lower cost. Electronic test results show that the time resolution of the TDC reaches 67 ps and the Effective Number Of Bits of ADC is better than 10.77 bit. The energy resolution of 511 keV photopeak is 4.1% and the Full Width at Half Maximum of the lifetime spectrum reaches 210.6 ps when using Hamamatsu H3378-50 Photomultiplier Tubes with $LaBr_3$:5% Ce^{3+} scintillators as detectors.

Keywords: Front-end electronics for detector readout, Spectrometers, Timing Detectors

[1]Corresponding author.

https://doi.org/10.1088/1748-0221/15/03/P03034

2020 JINST 15 P03034

Contents

2020 JINST 15 P03034

1 Introduction

Positron Annihilation Lifetime (PAL) spectroscopy has a wide application in material science and biomedical science. The β^+ source ^{22}Na emits a 1.28 MeV γ-quantum almost simultaneously with the positron generation and two γ-quanta of 511keV after the positron annihilates, which are treated as start and stop signals for the positron lifetime measurement, respectively [1]. The lifetimes of individual positrons are distributed as an exponentially decreasing function when annihilating in a constant electron density material. By measuring the lifetime spectra of bound states of the positron, one can study non-uniformity of materials, since the lifetime of probing bound states of positrons is changed by the presence of defects [2].

The most commonly used construction for PAL measurement is the fast-fast coincidence, as shown in figure 1 [3, 4]. The timing discriminators determine the arriving time of the Photomultiplier Tube (PMT) signals and set energy windows for the two detectors. The time interval between the start and stop signals is measured by Time-to-Amplitude Converter (TAC) and Multi-Channel Analyzer (MCA). The performance of the PAL spectrometer is restricted by the data processing capacity and measurement accuracy. Moreover, it is not easy to set up the system, typically composed by multiple standard Nuclear Instrumentation Modules (NIMs), due to its complex structure.

In recent years, the PAL spectrometer based on ultra-high-speed Analog-to-Digital Converter (ADC) or oscilloscopes has been developed to replace the bulky analog modules. The spectrometer has a simpler setup and achieves superior energy and time resolutions than conventional ones. However, it is hard to be widely applied for its performance strongly relies on the quality of the ADC or the oscilloscope [5–8]. Moreover, the two kinds of PAL spectrometers mentioned above usually cost tens of thousands of US dollars.

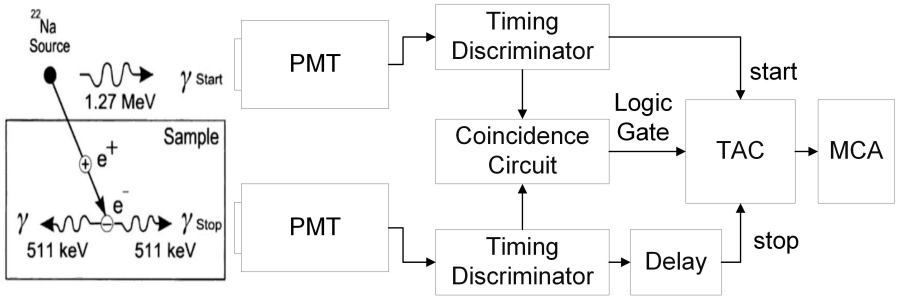

Figure 1. The structure of conventional fast-fast coincidence PAL spectrometer.

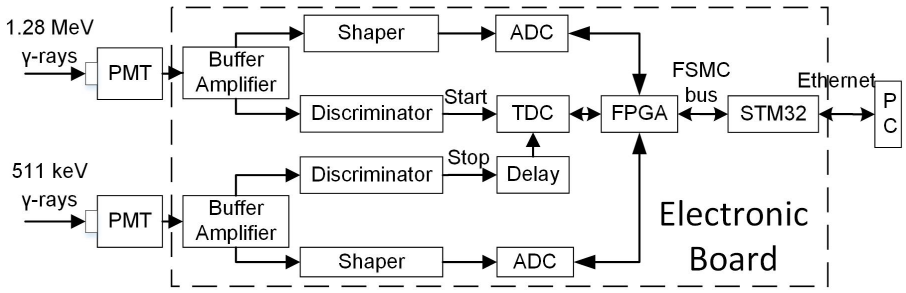

Figure 2. Block diagram of the electronic board.

In this paper we present a prototype system of a Time-to-Digital Converter (TDC)-based digital PAL spectrometer. Compared to the conventional PAL spectrometer and the digital PAL spectrometer based on ultra-high-speed sampling, the TDC-based PAL spectrometer has a simpler structure and much lower cost (less than 800 US dollars). The system achieves precise positron lifetime and energy measurements by employing the high-performance TDC and ADC. Besides, the application of a Field-Programmable Gate Array (FPGA) enhances the capability of the data process, such as peak search, time coincidence and filtering by photon energy. To verify the performance of the developed system, we conducted the electronic tests and the measurements of energy and lifetime spectra.

2 Electronic design

The electronic board consists of two buffer amplifiers, time and energy measurement circuits, an FPGA and the STM32 (a microcontroller with ARM CortexM3 core), as shown in figure 2. The buffer amplifier splits the input signal into two opposite-polarity single-ended signals for time and energy measurement respectively. The energy measurement circuit includes a shaper and an ADC. The time measurement circuit comprises two discriminators and a TDC. The Flexible Static Memory Controller (FSMC) bus connects the FPGA and the STM32. The STM32 communicates with Personal Computer (PC) via fast Ethernet. The electronic board contains 6 conducting layers. To reduce crosstalk, the routings and components of the energy and time measurement circuits are on different layers of the board.

2020 JINST 15 P03034

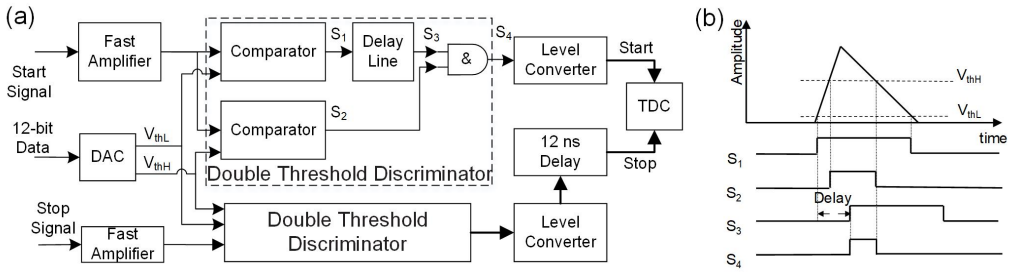

Figure 3. Block diagram (a) and the timing diagram (b) of the time measurement circuit.

2.1 Time measurement circuit

The block diagram of the time measurement circuit is shown in figure 3a. A commercial dedicated chip (ACAM GP2) is selected for the time measurement. The TDC-GP2 has a typical resolution of 65 ps, and the measurement range is [2 ns; 500 ns] in calibration mode [9]. The input signal is adjusted by a fast amplifier. A Double-Threshold Discriminator (DTD) is used to generate the start or stop signal for TDC. As shown in figure 3b, the low threshold (V_{thL}) discrimination signal S_1 passes a delay line to form signal S_3 and then coincide with the high threshold (V_{thH}) discrimination signal S_2 to generate the timing signal S_4. Typically, the time of signal arriving is determined by V_{thL}. The noise and some small signals can be rejected since signal S_4 will be high only when the signal amplitude exceeds V_{thH}. Compared to a single-threshold discriminator, one can select a lower V_{thL} to reduce the time walk [10]. The thresholds are obtained from a 12-bit, dual-channel Digital-to-Analog Converter (DAC) — MAX5234. To reduce the transmission delay and jitter, the Emitter Coupled Logic (ECL) devices are applied in the DTD circuit. Hence an ECL to Low Voltage Transistor-Transistor Logic level converter is needed to match the input level of TDC. The circuit of the stop channel is almost the same with the start signal, except a delay device with 12 ns delay added between the level converter and the TDC to guarantee that the time interval is in the TDC measurement range.

2.2 Energy measurement circuit

One of the buffer amplifier output is connected to the energy measurement circuit. The energy measurement circuit consists of 3 parts: a shaper (including a pole-zero cancellation circuit and a 2-stage RC filter), an ADC driver and an ADC, as illustrated in figure 4 [11]. To reduce pileup and increase pulse width, the input pulse is shaped into a 669 ns-width quasi-Gaussian wave by the shaper. The model of the amplifiers of the shaper is AD8007. A 14-bit, 125-MSPS dual-channel ADC — AD9648 digitizes the shaped signals of the 2 channels. Optimum performance is achieved while driving the ADC in a differential input by a full-differential ADC driver — LMH6550 [12].

2.3 FPGA firmware

We selected a high-performance and cost-effective FPGA — Altera Cyclone IV EP4CE30F484 to load the firmware of the system. The block diagram of the firmware is shown in figure 5.

After receiving both the start and the stop signals, the TDC measures and calibrates the time interval, and sends an interrupt signal to FPGA when the measurement is finished. Then the

2020 JINST 15 P03034

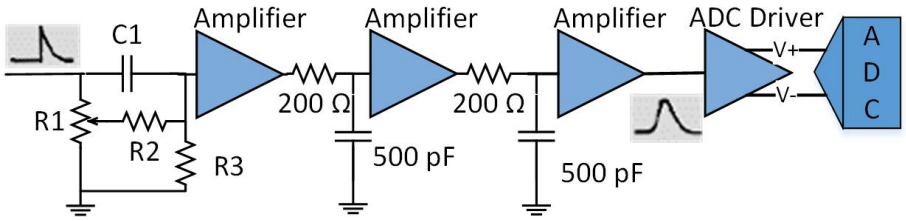

Figure 4. Schematic of the energy measurement circuit.

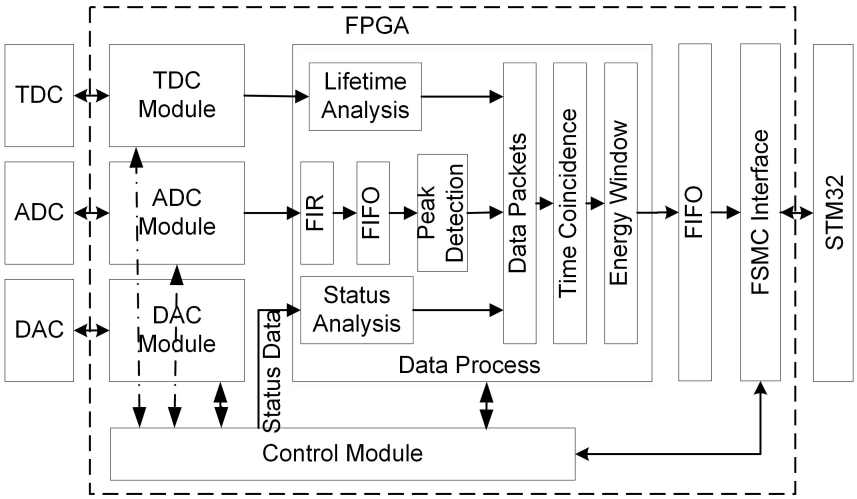

Figure 5. Block diagram of the FPGA firmware.

calibrated time data will be read by the FPGA. The ADC module acquires the waveform data of the shaped start and stop pulses. The Finite Impulse Response (FIR) low-pass filter with 5 MHz bandwidth is applied to further reduce the noise and smooth the waveform for peak searching. By comparing the value of 15 adjacent sampling points, the peak of the pulse can be detected. The maximum central point is decided as the peak value when the value of the 15 points increases first and then decreases. And we apply Newton's interpolation algorithm to correct the peak value for improving the accuracy [13]. The time, energy and status data of the same event will be packed in a data packet.

The function of coincidence is implemented in the FPGA to pick out the valid events. The time data should be in the range of the time window to ensure the relevance of events. To guarantee the exact 1.28 MeV-511 keV coincidence, the energy data of the start and stop signals should be distributed over the energy windows respectively. The events will be discarded if the time and energy data are not in the range of the windows. The time and energy windows can be set by the users. Compared to the analog coincidence methods in many conventional spectrometers, digital coincidence can be much more precise and flexible in events filtering and window settings.

All data packets of the coincidence events will be registered in First Input First Output (FIFO) and finally sent to STM32 via the FSMC bus.

2020 JINST 15 P03034

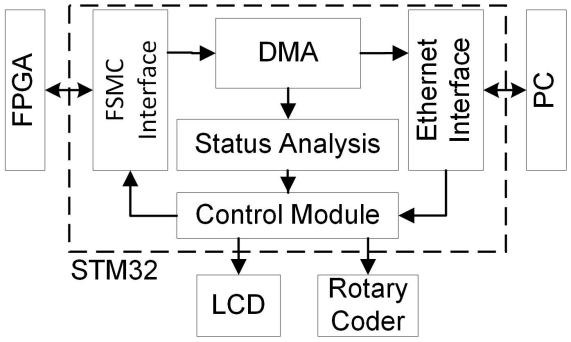

Figure 6. Block diagram of the STM32 software.

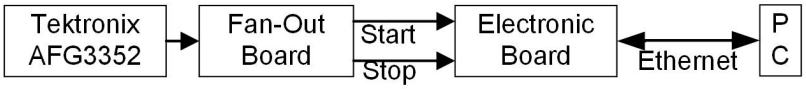

Figure 7. Block diagram of the time resolution test platform.

2.4 STM32 software

The system monitor can be achieved both on the PC and the local peripheral, such as Liquid Crystal Display (LCD) and rotary coder. A microcontroller STM32F207V6 is employed on the board for its advantages in display, manual control and TCP communication. The software block diagram is shown in figure 6. The STM32 receives the data from FPGA via the FSMC bus and then forwards it to the PC via Ethernet by Direct Memory Access (DMA). DMA allows the FPGA and the PC to transfer data directly without the involvement of the STM32 processor. The data rate from the FPGA to the PC can reach 20 MB/s. The STM32 acquires the system status from the data flow and updates the display every second. The fast Ethernet connects the board and the PC for the data and commands transfer.

3 Experiments and results

3.1 Electronic tests

Several electronic tests were carried out to evaluate the performance of the board, including the time and peak value measurement tests.

To test the time resolution of the electronic board, we used a signal generator Tektronix AFG3252 to generate a 100 Hz, 300mV and 50 ns-width pulse signal as the input signal. A fan-out board split the input signal into two as the start and stop signals respectively, as shown in figure 7. The additive phase jitter of the fan-out device IDT8SLVD1204I is less than 95 fs [14]. In this way, the relative jitter of the start and stop signals can almost be eliminated. After one hour of continuous measurement, the count histograms of the time interval between the start and stop were obtained, as shown in figure 8. The Gaussian fitting indicates that the time resolution reaches 67.30 ps.

To evaluate the linearity of the time measurement, we conducted the statistical code density test for the Integral Nonlinearity (INL) and Differential Nonlinearity (DNL). We used the two outputs of AFG3352 as the start and stop signals. The signals were 300 mV and 25 ns-width pulses and the

2020 JINST 15 P03034

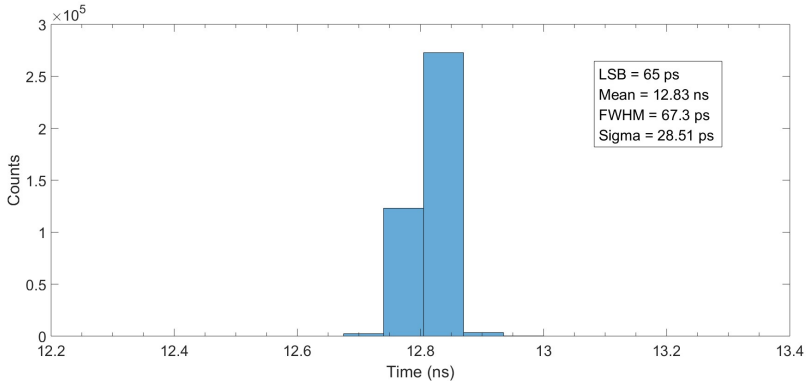

Figure 8. Typical count histogram of TDC at a specific delay.

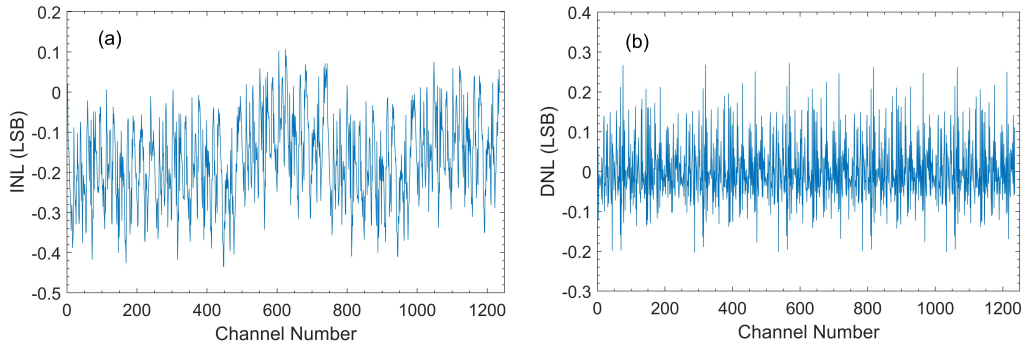

Figure 9. The INL (a) and DNL (b) of the time measurment.

frequencies of the start and stop signals were 567 Hz and 12.765 MHz. By analyzing the results of the code density, the INL and DNL of the time measurement can be obtained, which are in the ranges of [−0.43 LSB; 0.11 LSB] and [−0.20 LSB; 0.27 LSB] respectively, as shown in figure 9.

To test the dispersion of peak value measurement, we connected a 1 kHz, 165 mV and 50 ns-width pulse signal to each channel of the board. The histograms of the peak value counts of the start and stop channels are presented in figure 10. The mean value and the Full Width at Half Maximum (FWHM) of the fitting curve are about 8500 channels and 44 channels. The peak position and FWHM of 1.28 MeV photopeak measured by our spectrometer are 8478 channels and 229 channels (see figure 14). It can be calculated that the energy broadening caused by the detector is about 224 channels. The statistical broadening contributed by the electronic board is far less than that of the detectors in γ-ray energy measurement.

By changing the amplitude of the input signal and measuring the peak value of the shaped signal, the line chart of measured peak value vs. input amplitude can be drawn as figure 11. The linear fit result shows that the INL of the peak value measurement of the start and stop channels are 0.57% and 0.36% respectively.

A narrowband filter, whose center frequency and −3 dB bandwidth are 1 MHz and 0.1 MHz, was connected between the input of each channel and the 1 MHz, 370 mV sine wave source to reduce the external noise for the Effective Number Of Bits (ENOB) measurement. The frequency

2020 JINST 15 P03034

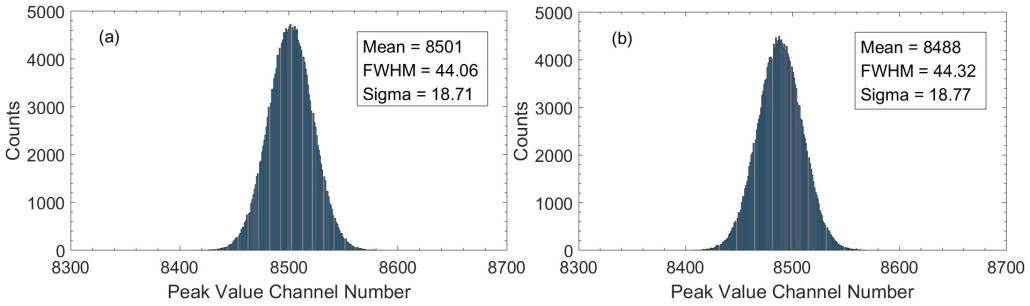

Figure 10. Peak value dispersion of each channel, (a) start channel, (b) stop channel.

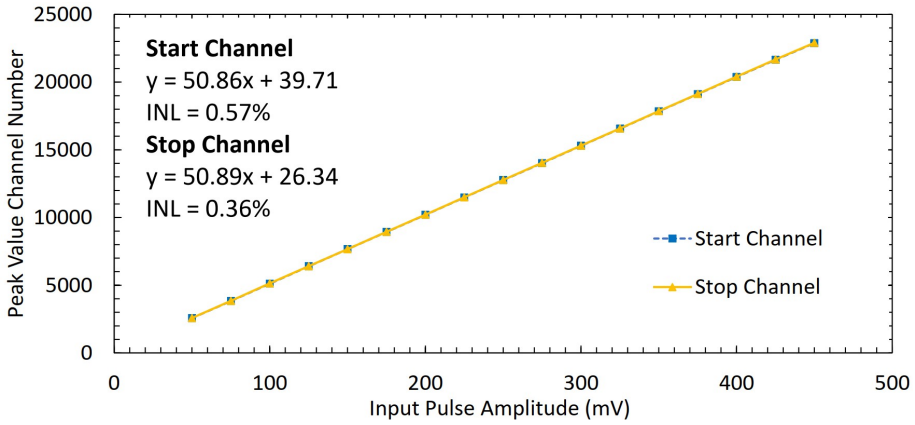

Figure 11. The linear fit of the measured peak value vs. input pulse amplitude

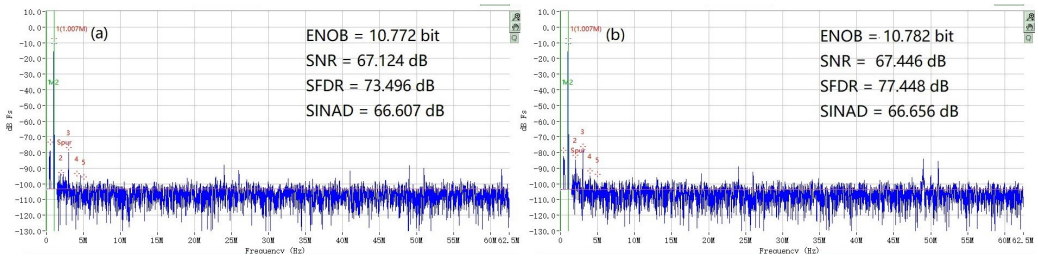

Figure 12. ADC sampling spectrum of each channel, (a) channel 1, (b) channel 2.

of the input was set as 1 MHz due to the limit of the shaping bandwidth. The signal amplitude after the shaper ranged from −830 mV to 960 mV, near full-scale of the ADC input. The ratio between Nyquist frequency and the shaping bandwidth would offer the opportunity for reduction of the noise thanks to oversampling and digital filtering. The sampling data were analyzed by Texas Instruments High-speed Data Converter Pro software for the spectra, as shown in figure 12. The results show that the overall ENOB is better than 10.77 bit.

3.2 PAL spectra tests

To verify the performance of the PAL spectrometer in actual nuclear applications, we carried out the PAL spectra tests with the test platform shown in figure 13. Two Hamamatsu H3378-50A PMTs,

2020 JINST 15 P03034

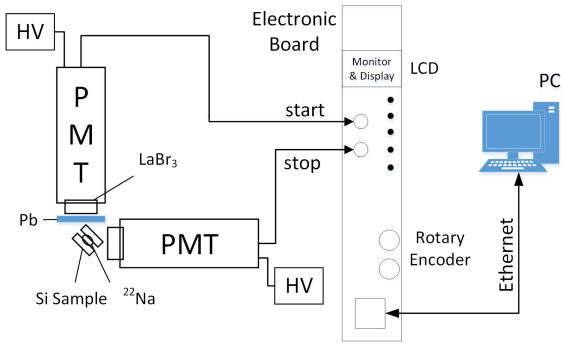

Figure 13. The structure of the PAL spectra test platform.

using Φ25 mm ×15 mm $LaBr_3$:5% Ce^{3+} scintillators, were biased with −1800 V High Voltage (HV) and adopted as the γ-ray detectors. The PMTs were placed at 90°. The radiation was emitted by a ^{22}Na source of nearly 740 kBq, which was sealed by Kapton films and sandwiched in the single crystal Si samples. The source was located at 5 cm in front of the detectors. A Pb slug was placed between the source and the start detector to block off the interference. The expected detection efficiency is about 0.005% [15]. Considering the geometrical coverage of the entire solid angle by the two PMTs, the Pb slug and the energy windows, the likelihood of coincidence efficiency should be about 30 cps.

Before the PAL spectra tests, we measured the noises of the electronic board and the PMTs by a Teledyne LeCroy wavesurfer 3104z 1 GHz-bandwidth oscilloscope with the probe. Firstly, we left the inputs of the board floating and measured the input noises of the discriminators of the two channels. The Root Mean Square (RMS) of the noise amplitudes were 1.20 mV and 0.90 mV, respectively. Then we connected the PMTs to the inputs of the board but removed the radioactive source to measure the combined noises of the PMTs and the board. The RMS of the noise amplitudes were 1.76 mV and 1.62 mV, respectively. At last, we put the radioactive source back and tested the input signals of the discriminators. The amplitude of the signals was mainly concentrated in the range of [200 mV; 1000 mV], which was far greater than the noises. We set the V_{thH} and V_{thL} to be 100 mV and 15 mV respectively according to the above test results.

To evaluate the performance of the energy measurement test, we disabled the time and energy window to acquire the energy information of all discriminated PMT signals. The energy spectrum was obtained by statistical analysis, as illustrated in figure 14. The energy resolutions of 511 keV and 1.28 MeV photopeaks reached 4.1% and 2.7%. According to the literature, the energy resolution of the Φ15 mm ×20 mm $LaBr_3$:5% Ce^{3+} scintillator at 662 keV is 3.58% when using 8 GS/s ADC for energy measurement [16, 17]. As the FWHM of the peak is almost inversely proportional to the square root of the deposited energy [18], it can be inferred that the energy resolution of our system at 662 keV is 3.59%, almost the same of the references. For more comparison, we tested the energy resolution by a set of conventional systems using the same detectors and ORTEC-572 amplifier [19]. The 511 keV photopeak energy resolution of the control group was 4.59%, worse than the result of our system.

The positron lifetime measurement was carried out by the electronic board with the PMTs at 90° arrangement (Setup 1). As aforementioned, the circuit structure and the coincidence logic

2020 JINST 15 P03034

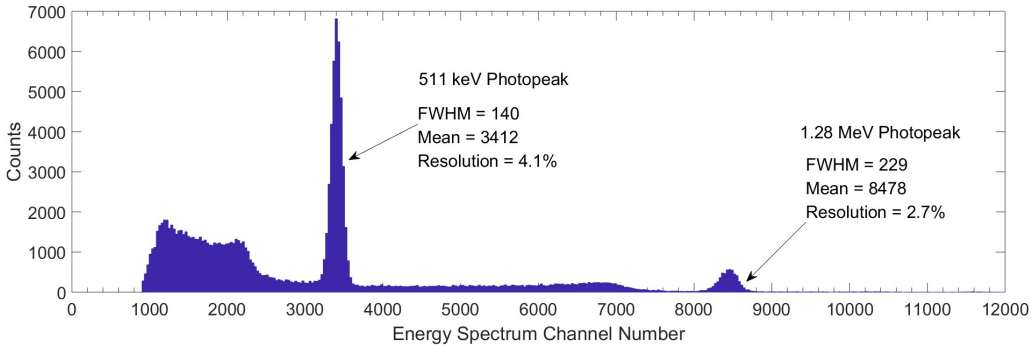

Figure 14. The energy spectrum of the start channel.

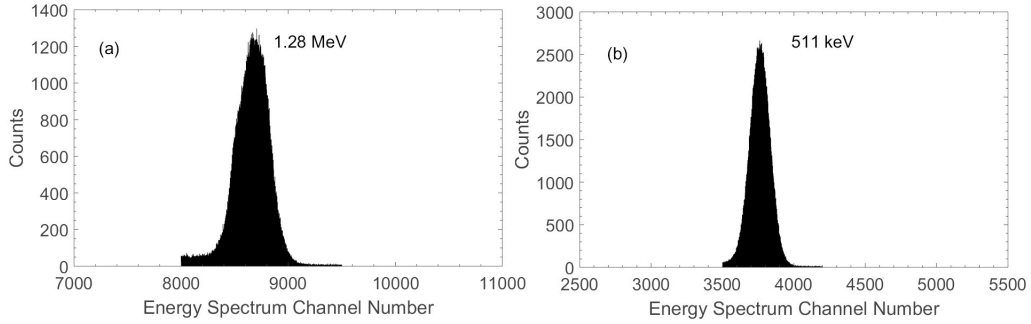

Figure 15. Energy spectra filtered by the energy window, (a) start channel, (b) stop channel.

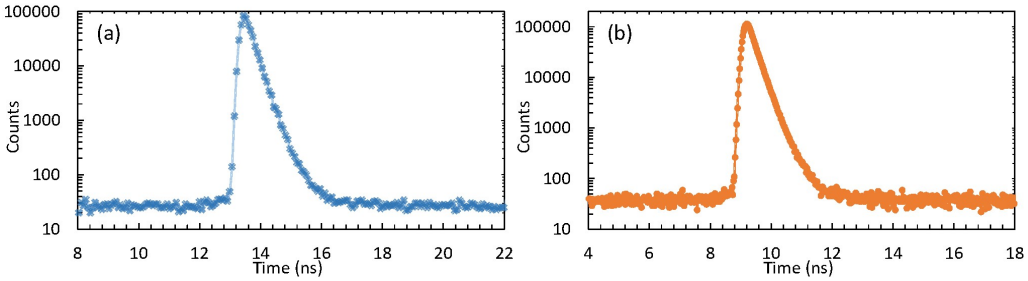

Figure 16. Lifetime spectra of Si sample (a) tested by setup 1, (b) tested by setup 2.

ensure that the valid events only occur when the start detector receives a 1.28 MeV γ-ray and the stop detector receives a 511 keV γ-ray in a short time. The time coincidence window was set to be [10 ns; 80 ns]. The average coincidence rate was 24 cps. After about 6 hours' measurement, we acquired the data of about 0.5 million valid events. The exact 1.28 MeV-511 keV γ-rays' coincidence events were picked out as seen in figure 15. The lifetime spectrum of Si sample measured by Setup 1 is shown in figure 16a.

We also conducted lifetime measurements using conventional commercial modules with the same detectors and radioactive source. The experimental Setup 2 is described in reference [19]. The lifetime spectrum of Si sample measured by Setup 2 is shown in figure 16b.

The lifetime spectra were analyzed by a generic positron lifetime analyzing software-Lifetime 9 (LTv9) [20]. The long lifetime component τ_3 is related to air-gap, NaCl salt or something else. As

2020 JINST 15 P03034

Table 1. Spectrum analysis results of the lifetime spectra tested by the two setups.

	τ_1 (ps)	I_1 (%)	τ_2 (ps)	I_2 (%)	τ_3 (ps)	I_3 (%)	FWHM(ps)
Setup 1	220.40 ± 1.6	86.47 ± 0.9	387.43 ± 5.7	12.44 ± 0.9	2(fixed)	0.09 ± 0.02	210.60
Setup 2	220.73 ± 0.9	87.50 ± 0.5	386.30 ± 2.2	12.39 ± 0.5	2(fixed)	0.10 ± 0.14	212.80

the intensity of τ_3 was less than 1%, we fixed τ_3 at an empirical value for the stability of the analysis results [19]. For Si sample, τ_1 and τ_2 should be about 220 ps and 385 ps with nearly 85% and 15% intensities, which are ascribed to the Si sample itself and the Kapton film [21]. The results tested by the PAL spectrometer constructed by the electronic board and the commercial modules are similar and fit the actual values well, as shown in table 1. The FWHM of the normalized full-chain timing response functions extracted from the fits to the lifetime spectra are 210.60 ps (Setup 1) and 212.80 ps (Setup 2) respectively.

4 Conclusion

The design and test results of the digital PAL spectrometer were presented. Compared to the conventional analog PAL spectrometer and recent ultra-fast-digitization based PAL spectrometer, the system employed high-performance TDC and ADC for time and energy measurement and reached competitive lifetime and energy resolution in a simple structure and at a much lower cost (less than 800 US dollars). The electronic test results state that the resolution and linearity of the time and energy measurement are good and in line with state-of-art setups. The time resolution of the electronic system reaches 67 ps and the ENOB of ADC is better than 10.77 bit. The energy measurement results indicate that the energy resolution (511 keV photopeak) of our system reaches 4.1% when using Φ25 mm $\times$15 mm $LaBr_3$:5% Ce^{3+} as scintillator, which is better than that of the conventional spectrometer (4.59%). The lifetime spectrum analysis results show that the FWHM of the timing resolution function is 210.6 ps. Compared to the conventional PAL spectrometer (the FWHM of the timing resolution function is 212.8 ps), the performance of our system in lifetime measurement is remarkable. It is much simpler to set up and more flexible to reconfigure our PAL spectrometer system than the conventional ones. In the future, we will do more work to improve the lifetime resolution of the digital PAL spectrometer based on TDC.

Acknowledgments

This work was supported by the National Natural Science Foundation of China under Grant No. 11527811. The authors would like to thank WANG Haibo, HAN Xiaoxi and YE Run for their support and suggestions in the experiments of the system. The authors thank XIANG Shitao for his guidance and help in the electronic design.

References

[1] R. Krause-Rehberg et al., *Positron annihilation in semiconductors*, Springer, Berlin Germany (1999).

[2] P. Hautojarvi et al., *Positron annihilation in solids*, Springer, Berlin Germany (1979).

2020 JINST 15 P03034

[3] C. Fong et al., *Positron annihilation lifetime spectroscopy (PALS): a probe for molecular organisation in self-assembled biomimetic systems*, *Phys. Chem. Chem. Phys.* **17** (2015) 17527.

[4] Y.C. Jean, *Positron annihilation spectroscopy for chemical analysis: A novel probe for microstructural analysis of polymers*, *Microchem. J.* **42** (1990) 72.

[5] F. Bečvář et al., *The asset of ultra-fast digitizers for positron-lifetime spectroscopy*, *Nucl. Instrum. Meth.* **A 539** (2005) 372.

[6] H. Saito et al., *A new positron lifetime spectrometer using a fast digital oscilloscope and BaF_2 scintillators*, *Nucl. Instrum. Meth.* **A 487** (2002) 612.

[7] L. Hui et al., *A simplified digital positron lifetime spectrometer based on a fast digital oscilloscope*, *Nucl. Instrum. Meth.* **A 625** (2011) 29.

[8] M. Petriska et al., *Positron lifetime setup based on DRS4 evaluation board*, *J. Phys. Conf. Ser.* **505** (2014) 012044.

[9] F. Dou et al., *A precise time measurement evaluation board for a radiography system of high-Z materials*, *Nucl. Sci. Tech.* **23** (2012) 284.

[10] A. R. Frolov et al., *Double threshold discriminator for timing measurements*, *Nucl. Instrum. Meth.* **A 356** (1995) 447.

[11] M. Cong et al., *Analog front-end prototype electronics for the LHAASO WCDA*, *Chin. Phys. C* **40** (2016) 16101.

[12] *AD9648 Datasheet*, https://www.analog.com/en/products/ad9648.html.

[13] F. Blais et al., *Real-time numerical peak detector*, *Sign. Proc.* **11** (1986) 145.

[14] *IDT8SLVD1204I datasheet*, https://www.idt.com/cn/zh/document/dst/8slvd1204i-datasheet

[15] S. Zhu et al., *γ-ray coincidence and fast-timing measurements using $LaBr_3(Ce)$ detectors and gammasphere*, *Nucl. Instrum. Meth.* **A 652** (2011) 231.

[16] M. Nakhostin et al., *Digital processing of signals from $LaBr_3$:Ce scintillation detectors*, 2014 *JINST* **12** C12049.

[17] E.V.D. Van Loaf et al., *Scintillation properties of $LaBr_3$:Ce^{3+} crystals: fast, efficient and high-energy-resolution scintillators*, *Nucl. Instrum. Meth.* **A 486** (2002) 254.

[18] G.F. Knoll, *Radiation detection and measurements*, John Willey and Sons Inc., New York U.S.A. (2000).

[19] L.H. Cong et al., *Reconfigurable positron annihilation lifetime spectrometer utilizing a multi-channel digitizer*, *Nucl. Instrum. Meth.* **A 946** (2019) 162691.

[20] J. Kansy, *Microcomputer program for analysis of positron annihilation lifetime spectra*, *Nucl. Instrum. Meth.* **A 374** (1996) 235.

[21] X. Ning et al., *Modification of source contribution in PALS by simulation using geant4 code*, *Nucl. Instrum. Meth.* **A 397** (2017) 75.

2020 JINST 15 P03034